



HAL
open science

Fine tuning of optoelectronic properties of single-walled carbon nanotubes from conductors to semiconductors

Zeinab El-Moussawi, Ali Nourdine, Hussein Medlej, Tayssir Hamieh, Pascale Chenevier, Lionel Flandin

► To cite this version:

Zeinab El-Moussawi, Ali Nourdine, Hussein Medlej, Tayssir Hamieh, Pascale Chenevier, et al.. Fine tuning of optoelectronic properties of single-walled carbon nanotubes from conductors to semiconductors. *Carbon*, 2019, 153, pp.337-346. 10.1016/j.carbon.2019.07.023 . hal-02192786

HAL Id: hal-02192786

<https://hal.science/hal-02192786>

Submitted on 25 Oct 2021

HAL is a multi-disciplinary open access archive for the deposit and dissemination of scientific research documents, whether they are published or not. The documents may come from teaching and research institutions in France or abroad, or from public or private research centers.

L'archive ouverte pluridisciplinaire **HAL**, est destinée au dépôt et à la diffusion de documents scientifiques de niveau recherche, publiés ou non, émanant des établissements d'enseignement et de recherche français ou étrangers, des laboratoires publics ou privés.



Distributed under a Creative Commons Attribution - NonCommercial 4.0 International License

Fine Tuning of Optoelectronic Properties of Single-Walled Carbon Nanotubes from Conductors to Semiconductors

Zeinab El-Moussawi^{1,2}, Ali Nourdine^{1*}, Hussein Medlej², Tayssir Hamieh², Pascale Chenevier³, Lionel Flandin¹

¹Univ. Savoie Mont Blanc, CNRS, G-INP, LEPMI, Chambéry, 73000, France

²Univ. Libanaise, MCEMA laboratory, Campus Rafic Hariri, Hadath, Lebanon

³INAC, SPRAM, CEA Grenoble, F-38000 Grenoble, France

KEYWORDS: SWNT, conductor, semiconductor, functionalization, optoelectronic, conductivity.

Abstract:

Controlling both conductivity and bandgap chemistry of carbonaceous fillers could broaden up their application potential. However, it has been a difficult synthetic goal for more than a decade. We describe a methodology to do so in a very controlled manner on single-walled carbon nanotubes (SWNT). The approach relies on the extreme extension of a functionalization by 4-nitrobenzenediazoether. We show that the water-soluble Z-diazoether already known to react selectively with metallic m-SWNTs, can also extract electrons from sc-SWNTs. The gradual formation of a covalent aryl bond alters the SWNT electrical conductivity in two steps depending on the functionalization degree. The two consecutive regimes correspond to the grafting of conductor and semiconductor nanotubes. The extent of functionalization was assessed in situ using UV-Vis spectroscopy. The covalent coupling was first evidenced by spectroscopic characterizations of the chemical structure. The consequences on the physical properties of the SWNTs were also measured. The functionalization method reported here brings unprecedented hope for preparing, at large scale, semiconducting SWNTs as excellent-conductivity building blocks for an array of applied semiconductors. This is the first example of the visualization and measurement of optical and electrical properties in function of the progress of nitrophenyl coupling to nanocarbon scaffolds.

1. Introduction

CNTs are organic molecular cylinders produced as polydisperse mixture of metallic and semiconducting materials. The comprehensive range of unique mechanical, thermal, chemical, optical and electrical properties of CNTs has made them a potential tool of interest since their discovery.[1] With the dawn of nanotechnology now unfolding, many potential applications have been proposed for carbon nanotubes, including conductive and high-strength composites, energy storage and energy conversion media, sensors, supercapacitors, field emission displays and nanometer-sized semiconductor devices.[2, 3] Some of these applications have reached high TRL. Others are demonstrated in early to advanced devices, and some, semiconductor devices, are clouded by controversy.

For example, one of the most successful applications to CNTs is their incorporation into otherwise insulating materials, with the aim to help composite materials truly take advantage of their outstanding electrical properties.[4, 5]

However, due to their high intrinsic conductivity and imprecise assembly, pristine carbon nanotubes are unsuitable for direct implementation or scale up in electronic and optoelectronic applications.[6] Reports therefore note a negative effect of metallic conductivity in semiconductor-based nanoelectronics like field-effect transistors and organic solar cells[7, 8] where metallic conductivity is at the origin of low on/off ratios and induces short circuits, respectively.[9] In biomedical also, even subtle heterogeneities can dramatically hinder the device performance.[10]

Related with this, powerful experimental approaches like selective electrical heating of metallic SWNTs,[2] electrophoresis,[11] density gradient ultracentrifugation[12, 13] and chromatography,[14] have been proposed to sort, isolate, functionalize or separate CNTs into two electronic types, partially mending their incompatibility and making their use possible in some of the most promising applications. If the above methods minimize or eliminate the undesirable effects of metallic CNTs on the required functional properties, a key common drawback remains high prices or time consuming procedures that would, combined to a low efficiency, limit the practical applicability in a scalable manner. Therefore selective chemical reactions have been developed in a similar context.[15, 16]

Covalent sidewall functionalization offers another possible route to SWNT sorting, via linking addends to sidewall carbon atoms of the nanotube.[17, 18] It was reported that metallic SWNTs can react with aryldiazonium salts to near exclusion of the semiconducting chiralities.[19-24] Recently, 4-nitrobenzene diazoether has shown an unprecedented selectivity to m-SWNTs inasmuch as it is added in small amounts.[25, 26] Compared to semiconductors, metallic carbon nanotubes possess more electrons near the Fermi level,[24] and are thus more amenable to initiate the covalent bond formation with the electron withdrawing nitrophenyl (NP) functional group. In another significant work, and using the same NP addend, the reaction selectivity was achieved with semiconducting SWNTs at a higher chirality-selective level.[27]

In spite of the longstanding efforts of researchers to develop new functionalization routes, approaches remain non controllable and do not tailor the electrical properties in function of linked addends, except in niche situations,[17, 28, 29] and, in one example, fluorination at 250 °C was detrimental to CNT conductance where nanotubes became totally insulating.[30]

More functionalization methods are duly needed, which combine the control of functionalization degree with experimentally measured intrinsic properties, electrical and optical. They should be simple, effective and cost-effective to allow easy scale up for possible industrial technologies. With such applications in mind, we present, in the current study, some functional examples for covalently tailored SWNTs obtained by varying the injected amounts of 4-nitrobenzenediazoether. The UV-Vis spectroscopy was used as a sensitive, quantitative indicator of functional degree and to monitor, at the same time, the surface chemistry of SWNTs in situ. Raman was also conducted on the final products to estimate the functional degree. The nitrophenyl-functionalized SWNTs (NP-SWNTs) are stable in solution and have been characterized by a number of spectroscopic and microscopic techniques, including UV-Vis-NIR, Raman and impedance spectroscopies, transmission electron microscopy and scanning electron microscopy. The functionalization of sc-SWNTs beyond only metallics, here denoted as superfunctionalization, has a limit that corresponds to either a steric hindrance and/or *a posteriori* poor electron density. Absolute differences in functional degree of carbon nanotubes led to marked changes in the conductivities of these species, although largely overlooked in previous studies. We record for an addition of 15 nitrophenyl (NP) to 100 carbon atoms (i.e., 31 NP/100 double bonds, 46 NP/100 SWNT rings or 61 wt.% NP/SWNT), a 34000-fold lower conductivity as opposed to non-functionalized carbon nanotubes with a conductivity value of $\sim 10^{-4}$ S/m. This on-demand conductivity has not been previously reported and is a target value for the aforementioned applications. To illustrate this concept, we ultimately model the number of existing double bonds with the functionalization progress. The strong structure dependence of the macroscopic optical and electrical properties suggests an approach for scalable nanomaterials with on-demand properties. We noticed that the functionalization of SWNT facilitates the dispersion of SWNT in polar and non-polar solvents without surfactants. This qualitative effect increases with higher functionalization degrees and correlates qualitatively with the reduced number of sp^2 -hybridized carbon

atoms in the hexagonal lattice. The potency to use wet-processing methods to fabricate and/or integrate functionalized CNTs into thin film devices, paves the way to the rational design, and further the true production of devices over large areas using roll-to-roll or printing techniques, in which the interaction of the solvent with the nanotube surface chemistry plays an important role.

2. Results and Discussion

2.1. Superfunctionalization of SWNT using 4-nitrobenzene diazoether

The gradual grafting of nitrophenyl addends onto CNT metallic surfaces to the exclusion of the semiconductors has proved successful with a host of characterization techniques. Under carefully controlled conditions, this behavior can be exploited to obtain SWNT with highly selective conductivities. In contrast with previous works reporting the effect of functionalization on free standing nanotubes, which do not necessarily represent the sample as a whole due to SWNT inherent structural differences, we took special care to determine the macroscopic effects on the intrinsic properties of a bulk CNT sample (buckypaper or thin film) including electrical conductivity, optical absorption and electrochemical bandgap. Therefore electrical and optical properties of pristine and chemically modified SWNTs, buckypapers or thin films, were thoroughly characterized. Table 1 summarizes a set of seven functionalization degrees expressed in NP weight percentage (NP wt.%) as determined by two techniques, UV-Vis-NIR and Raman. To obtain the latter wt.%, a retro-analysis of the ID/IG ratio extracted from Raman on the final product is used. For precision, each Raman-based functional degree is expressed in equivalents like number of NP addends per 100 SWNT carbon atoms (NP mol.%-C), 100 aromatic rings (NP mol.%-AR), and 100 double bonds (NP mol.%-DB). The corresponding electrical conductivities are also

mentioned. These values show a conductivity offset of ~ 34000 between pristine SWNT and the uppermost functional degree (NP-SWNT-61).

Table 1. Chemical composition and electrical conductivity of the functionalized SWNT samples (NP-SWNT-X), where X is the weight percentage of nitrophenyl in SWNT. The corresponding electrical

| Nomenclature NP-SWNT- wt.% ^a | ID/IG | NP/SWNT- Raman ^a (wt.%) | NP/SWNT- UV/Vis ^b (wt.%) | NP/100C (NP mol.% -C) Raman-UV/Vis | NP/100DB (NP mol.% -DB) Raman-UV/Vis | NP/100AR (NP mol.% -AR) Raman-UV/Vis | Electrical Conductivity ^c σ (S/m) | Inverse of rela- tive electrical conductivity ^d | Electrical character |
|--|-------|--|---|--|--|--|---|--|-------------------------|
| SWNT | 0.06 | 0 | 0 | 0-0 | 0-0 | 0-0 | 13.5 \pm 0.5 | 1 | conductor |
| NP-SWNT-7 | 0.08 | 7.00 | 16.7 | 0.7-3.8 | 1.4-7.6 | 2.2-11.4 | 3 \pm 1 | 5 | |
| NP-SWNT-14 | 0.10 | 14.0 | 25.5 | 1.6-6.3 | 3.2-12.6 | 4.8-18.9 | 2.3 \pm 0.8 | 6 | |
| NP-SWNT-21 | 0.12 | 20.4 | 37.5 | 2.6-10.5 | 5.2-21.0 | 7.6-31.5 | 1.5 \pm 0.5 | 9 | conductor |
| NP-SWNT-49 | 0.31 | 49.0 | 66.5 | 9.5-28.1 | 19.0-56.2 | 28.4-84.3 | 0.12 \pm 0.02 | 113 | semi-conductor |
| NP-SWNT-54 | 0.37 | 53.6 | 66.5 | 11.5-28.1 | 23.0-56.2 | 34.0-84.3 | 0.08 \pm 0.02 | 169 | |
| NP-SWNT-56 | 0.42 | 56.3 | 66.3 | 12.7-27.9 | 25.4-55.8 | 38.0-83.7 | 0.03 \pm 0.02 | 451 | |
| NP-SWNT-61 | 0.53 | 61.0 | 68.1 | 15.4-29.6 | 30.8-59.2 | 46.1-88.8 | (4 \pm 2.5) 10 ⁻⁴ | 33825 | |

behavior is equally mentioned.

^aNP/SWNT (wt.%) deduced from Raman spectra (equation S1 in supplementary information).

^bNP/SWNT (wt.%) estimated from UV-Vis spectra (figure S3 in supplementary information).

^cConductivity measured according to the conditions described in experimental section.

^dInverse of relative electrical conductivity $1/\sigma_{rel} = \sigma_{SWNT}/\sigma_{NP-SWNT-X}$.

2.2. Chemical structure and composition of NP-SWNT-X

Figure 1a shows the UV-Vis-NIR absorption spectra of DMF suspended nanotubes after successive additions of 4-ascorbate diazoether, washing and filtration. Measuring solution absorption features after powerful sonication of functionalized SWNT in DMF allows for the monitoring of

the covalent nature of nitrophenyl coupling at each distinct functional degree. Solution concentration was fixed at 0.1 g/L. In Figure 1b we recorded the relative quenching of S22 and M11 peak maxima respectively at 954 and 651 nm. Baseline-corrected spectra monitor that metallic (M11) transitions initially decay, in response to the electron localization as the species react to form covalent linkages and are as a result no longer free to participate in photoabsorption. The functionalization of all metallic nanotubes, denoted here as metallic threshold, corresponds to 21 wt.% of NP. Above the so-called threshold S22 starts to decay gradually while M11 intensity keeps nearly constant. With S33, the signal intensity was, as expected, not altered by the initial selective functionalization of m-SWCNT (NP-SWCNT-21). In contrast a significant attenuation of S33 was detected beyond this critical value, and related the functionalization of sc-SWCNTs. As shown in Figure 1b, An almost total semiconducting decay is obtained for the highest functionalization degree 61 wt.%. The minimal absorption attained here corresponds to the limit of functionalization. Further reagent addition does not lead to more decay in absorption intensities nor to higher functionalization densities probably because of steric effects, site saturation, gradual decrease on the reactivity of pre-functionalized SWNTs vs. NP reactivity with the functionalization progression, and total deactivation of SWNTs.

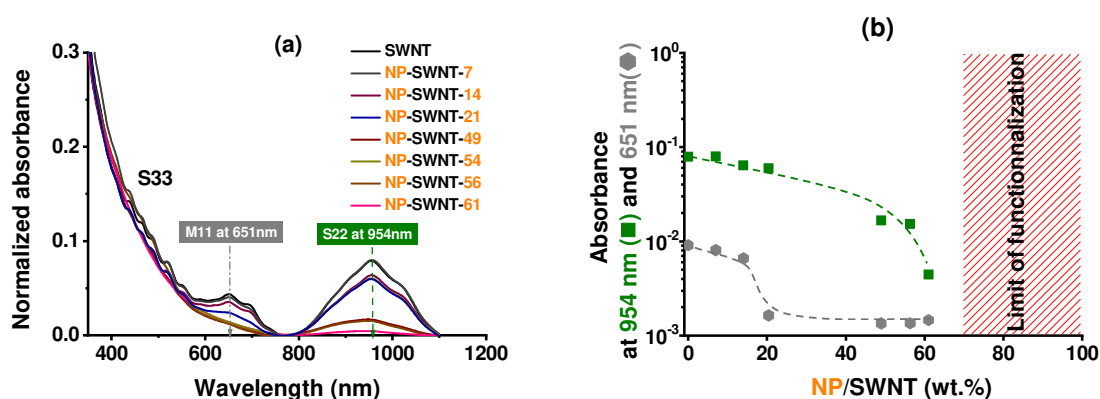


Figure 1. Solution absorption spectroscopy of SWNT and NP-SWNT dispersed in DMF solutions. **(a)** Spectra of NP-SWNT redispersed in DMF confirm their covalent linkage to NP groups. The heavily tethered carbon nanotubes (pink) have almost lost all van Hove transitions, whereas the electronic properties of the other fractions are retained in different percentages. **(b)** Relative absorption peak heights at wavelengths of 954 (green) and 651 nm (grey) in function of 4-nitrobenzene diazoether quantity for aligned spectra between 780 and 1100 nm.

Figure 2a compares the Raman spectra at excitation length of 532 nm before and after functionalization. This wavelength was used because it probes both metals and semiconductors. The spectra comprising both electronic transition modes, D and G band which depend only on the hybridization state of carbons in C-C bonds,[31] are nearly similar in absence of and at low functionalization degree. However the top trace (NP-SWNT-61) shows an intense D band near 1300 cm^{-1} , induced by conversion of $\text{sp}^2\text{ C}$ to $\text{sp}^3\text{ C}$ on the nanotube during the formation of C nanotube aryl bond.[32] The Raman signal is normalized for pristine carbon nanotubes to the maximum intensity of unity. The plot of ID/IG band peak intensity ratio, also corresponding to the ratio of C-C simple bonds introduced into the carbon lattice, allows to calculate the ratio of remaining double bonds and to consequently identify the nitrophenyl weight percentage in SWNTs. (See supplementary information for calculation details). In Figure 2b the Raman-based NP-wt.% deduced from ID/IG band peak intensity ratio, varies linearly with the functional degree calculated from the UV-Vis-NIR spectra. The typically higher wt.% calculated from UV-Vis (Figure 2) could originate mainly from differences in the measured media as well as the means of signal detection. In Raman, we measure the ID/IG response of the functionalized nanotubes in films. In UV, however, the E iso-

mer is dosed in liquid media, and used to estimate the Z-intake and deduce the amount of NP addends linked to the nanotubes surface (See supplementary information for calculation details).

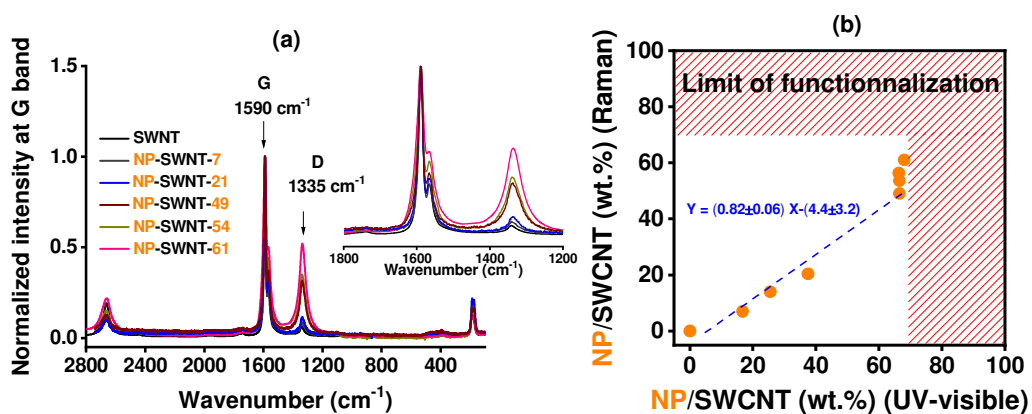


Figure 2. Resonant Raman spectra on SWNT and NP-SWNT thin films drop-coated from liquid suspensions in DMF. **(a)** Low-wave number Raman spectra at 532-nm excitation of the SWNT and NP-SWNT-X at different functional degrees. Raman intensities were normalized to that of the G band for comparison. Inset shows a zoom of D and G bands at 1339 and 1589 cm^{-1} respectively. **(b)** Correlation between Raman-based and UV-based nitrophenyl wt.%. A linear relationship with a slope close to 0,82 is obtained.

The presence of NO_2 groups on the NT surface is analogously confirmed by FT-IR spectroscopy (Figure 3). Though difficult to detect at low functional degrees, the spectra of heavily nitrophenyl-functionalized SWNTs exhibit new bands corresponding to spectroscopic signatures of the symmetric and asymmetric stretching modes of NO_2 group at 1540 and 1356 cm^{-1} , respectively. We

realized that the stretch initially at 1540 cm^{-1} was shifted towards lower wavenumber.[33] This probably results from the increasing surface coverage with NP addends. This measurement indicates a substantial dependence of macroscopic properties on sp^2 carbon chemistry that varies tremendously with the functionalization density.

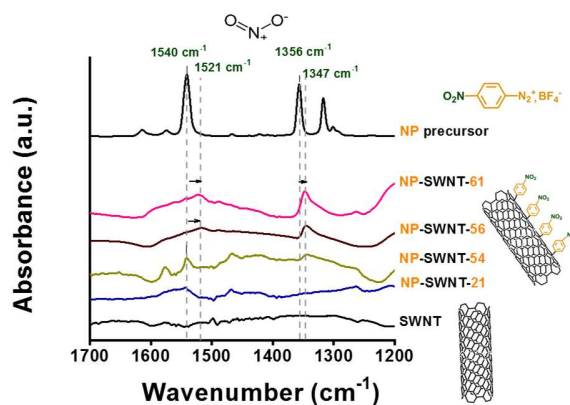


Figure 3. Effect of superfunctionalization on the surface chemistry of SWNTs: ATR FT-IR spectra of pristine and NP-functionalized SWNTs. The nitrobenzene diazonium tetrafluoroborate is shown for comparison.

2.3. Dispersibility, nanostructure of functionalized and superfunctionalized SWNT (SWNT-X)

Extended structure modification of CNTs *via* super-functionalization has dispersing effects even in the solid state (Figure 4a). SEM micrographs of DMF-casted films reveal that superfunctionalization facilitates the nano-dispersion in organic media and reduces the tendency to aggregate especially at elevated functional degrees because of the decreased number of π - π and Van der Waals interactions between SWNT particles. The average bundle size decreases from 47 to 10 nm, sug-

gesting the presence of 8 NTs instead of 39 per bundle (Figure 4b). NTs could be more or less individualized depending on the bundle size. Statistics on NP-SWCNT-61 images reveal bundles containing only two SWNTs. This is in accordance with the decrease in the intrinsic viscosity due to decreased bundle size after functionalization (see Figure S4 in Supplementary information).

TEM microscopy of the resulting SWNTs shows the NPs assembled along the sidewall of the SWNTs (Figure 5). The higher the functionalization degree, the denser the NP layer, and indeed the comparison with the pristine NT morphology suggests a semi-continuous NP layer attached to the surface of CNTs in a core-shell manner. The diameter of two SWNTs in the most functionalized sample is 1.16 times higher than for pristine (uncoated) tubes. We find that the external nanotube walls exhibit more rumpled structure as functionalization becomes more important.

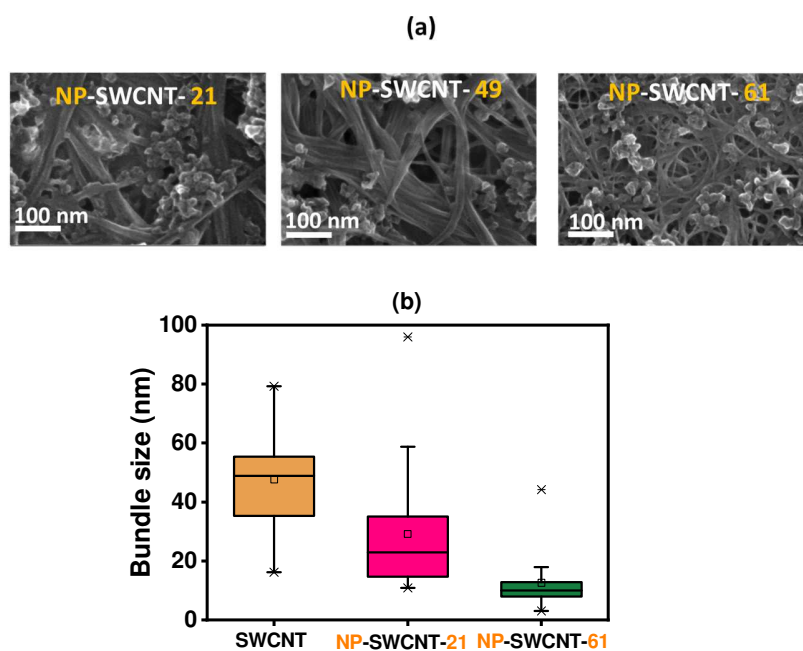


Figure 4. How super-functionalization favors SWNT dispersibility? (a) SEM images of thin NP-SWNT films drop-casted from dilute DMF solutions. (b) Superfunctionalization decreases the size of NT bundles.

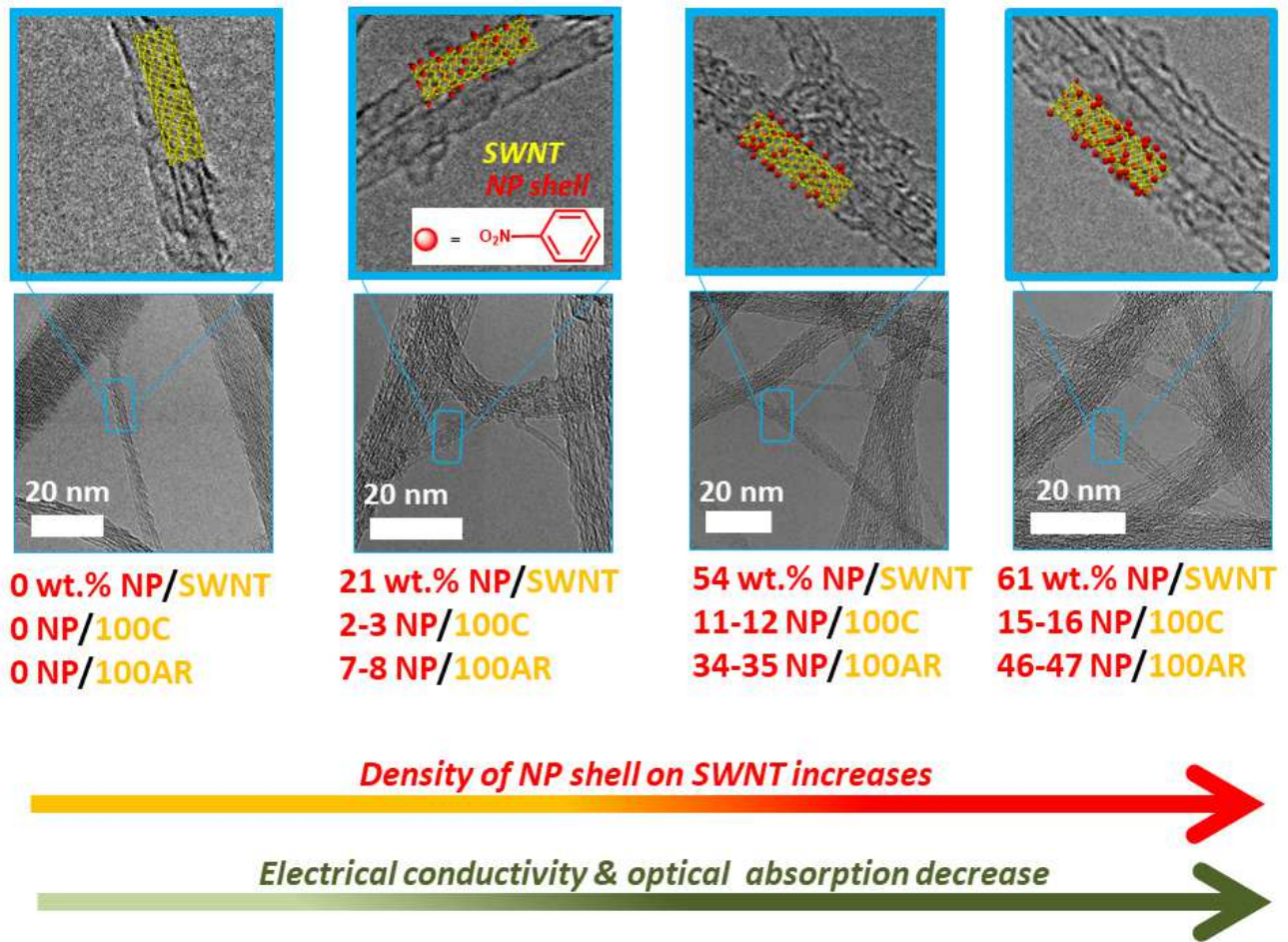


Figure 5. Representative TEM micrographs (from left to right) of pristine SWNT, NP-SWNT-21, NP-SWNT-54 and NP-SWNT-61.

2.4. Effect of extended nitrophenyl –SWNT coupling on optical properties

Figure 6a indicates the thin film UV-Vis-NIR absorbance of control and other functionalized SWNT samples. Akin to solution suspensions, spectra of homogeneous films show a distinct gradient of optical properties in UV (262 nm), visible (570-750nm) and IR (954 nm) zones. A decrease in plasmon peak and removal of transition bands reflect tailored π -network SWNT disrupting, and functionalized spectra gradually lose the complexity of electronic structure, compared with pristine materials. In order to more precisely identify the poorer curve morphologies for NP-SWNTs with the progress of functionalization, we traced in Figure 6b the absorptivity of π - π plasmonic peak at 262 nm and the semiconductor peak at 954 nm, in function of the functional degree NP-wt.%. In order to avoid errors that may arise from the contribution of nitrophenyl group to the sample weight, we defined a specific absorption coefficient that takes into account the nitrophenyl weight percentage in SWNTs, and the values were accordingly corrected. Spectra were matched in baseline to allow quantitative comparisons. The gradual loss of conjugation length can be inferred from the first transition peak. ϵ -262 nm that reflects π - π^* transition in NTs, evolves in two steps. The first ends at the metallic threshold, and a second step occurs during the functionalization of sc-SWNTs then becomes nearly constant at NP wt.% = 56; before the functionalization limit. The specific absorption coefficient relative to sc-SWNTs ϵ -954 nm does not show important variation however at low addend densities i.e. before the metallic threshold, due to the reaction selectivity. A much sharper dependence on the functionalization degree is revealed between 21 and 56 NP-wt.%, where tethering of nitrophenyl groups to sc-SWNT surface reduces there absorption signature to a minimal value of $3.7 \text{ L g}^{-1} \text{ cm}^{-1}$. Between 56 and 61 wt.%, the absorptivity values are quite similar, despite a 2-fold decrease in electrical conductivity (Figure 7), which may be attributed to the effect of nanotube coulomb interactions that hinder closer detection of optical properties using UV-Vis-NIR spectroscopy.

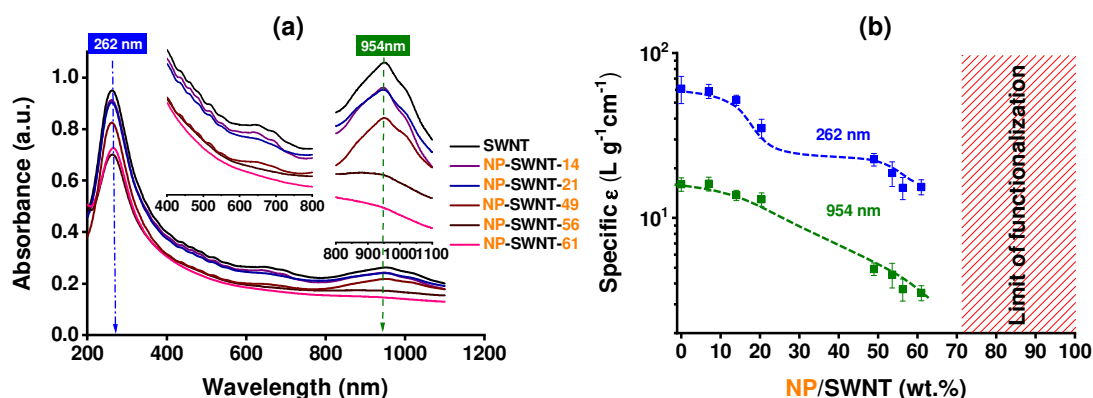


Figure 6. UV-Vis-NIR spectral data illustrating the evolution of absorption for pristine and functionalized materials. **(a)** Absorption spectra of SWNT on quartz substrates in thin films normalized to 100 nm. **(b)** A plot of both specific extinction coefficients at 262 nm and 954 nm with the functionalization degree.

2.5. Effect of extended nitrophenyl-SWNT coupling on electrical conductivity

Another view of this pattern can be seen in Figure 7, where we plot conductivities of a set of nitrophenylated SWNT samples at widely spaced functional degrees. We did verify reproducibility issues[20] in the early stages of this investigation, and we have identified at least two samples for a credible measure. The bottom scales show the numbers of NP addends per nanotube carbon atom, nanotube double bond or nanotube aromatic ring, all derived from the mass percentages plotted underneath. The plot shows 2 dropping steps. The first transition corresponds to the functionalization of m-NTs; the conductivity initially measured 13.5 S/m, decreases systematically as the functional degree is increased till 21 wt.%. Then the onset of semiconductors functionalization is accompanied by a slightly inclined

plateau then a particularly sharp sigmoidal drop between 54 and 61 wt.%. The presence of two distinguishable transitions points to non-similar mechanisms depending on the character of the target NT to be functionalized. We interpret the overall conductivity changes as reflecting the gradual destruction of the extended π -network, thereby the disruption of the translational symmetry and changing the electronic structure of the SWNTs. Also, the presence of aryl groups at the surface of m and sc-SWNTs probably prevents close SWNT-SWNT contact and fast electron conduction. Covalently functionalizing SWNTs thus offers a novel controlled, non-destructive way to tailor the optoelectronic properties of nanotubes. Treatment of carbon nanotubes by NP group, which resembles to a certain extent a depercolation phenomenon, reduces the conductivity to $4 \cdot 10^{-4}$ S/m, a typical value for many optoelectronic applications. Through NP coupling we gradually reduce the conductivity by 4 orders of magnitude and modulate light absorption by SWNTs. NP-SWNTs could lead to voltage-switchable dielectric materials having conductive or semiconductive properties.

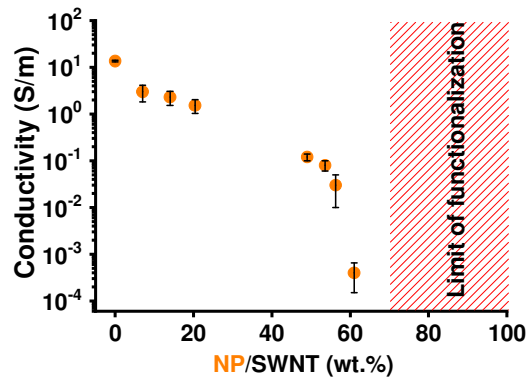


Figure 7. Electrical conductivity versus degree of functionalization.

In order to better understand the electrical performance of NP-SWNTs over the extent of functionalization, AC impedance measurements were carried out on buckypapers. Nyquist plots and corresponding

equivalent electrical circuits are shown in Figure 8a, and extracted data are plotted in Figure 8b. Between no functionalization and the metallic threshold (NP-SWNT-21), resistivity increases monotonically and materials are conductors with vertical plots and modeled in a single resistance.

As diazoether superfunctionalization proceeds, the equivalent circuit could be represented using the RRC model between 10^{-3} and 10^9 Hz. Here materials start to exhibit semiconducting character in the order of 10^{-2} S/m. Beyond NP-SWNT-56, we have a real semiconductor that obeys R1/C1 model with $R1 = 10^4 \Omega.m$. It is worthy to mention the excellent agreement of conductivity values estimated by the impedance models with those experimentally extracted from I-V curves (Figure 8b). The decrease in metallicity of SWNT and introduction of capacitance, and indeed its evolution with the extent of functionalization, can be mainly attributed to the incorporation of NP addends. First these addends act physically as spacers that reduce the local NT-NT contact minimizing the electrostatic interaction and hindering electron transport from one tube to another. Second, the initially free charges to move are less mobile and moreover trapped between NP-NTs increasing the local stored electron density, increasing the capacity.[34]

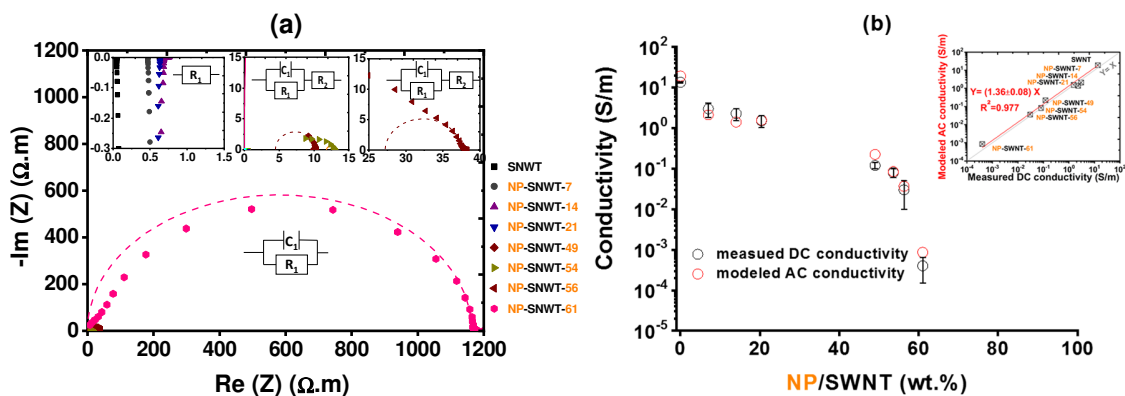


Figure 8. (a) Nyquist diagrams of pristine and functionalized SWNTs and equivalent circuit models. **(b)** Compatibility between experimentally measured conductivity (red circles) and modeled data (black circles).

2.6. Electrical depercolation in functionalized and superfunctionalized NP-SWNT-X

SWNTs can be a strong material for electrical percolation in otherwise insulating composites and percolation thresholds have been extremely studied in literature.[35, 36] In this study, the depercolation of functionalized carbon nanotubes, the inverse phenomenon, is investigated as the number of double bonds decreases in the hexagonal lattice. The depercolation accounts for the remaining ratio of double bonds in the sample after each addend addition (Figure 9a). At the metallic threshold, only 5% of the double bonds are functionalized. We noticed that conductivity diminishes linearly when m-NTs are grafted, then diverges downward, as semiconductors are grafted, to $4 \cdot 10^{-4}$ S/m. The S-shaped curve suggests that sc-SWNTs lose conductivity in a depercolation mechanism, but m-SWNTs do not do so. It is most probable that when only metallics are grafted, the measured conductivity is highly influenced by the surrounding intact double bond network of sc-SWNTs, the reason behind the conductor character is still predominant. On the other hand, when sc-SWNTs are functionalized, no “parasitic” conjugation will affect the measurements because metallic species are already functionalized. The mechanism could be also different because it is more difficult to initiate the functionalization for sc-SWNTs due to inherent lower electron density compared to metallics and deeper HOMO level.[25]. Universal Kirkpatrick’s percolation law[37] $\sigma = \sigma_0 \cdot (\Phi - \Phi_c)^t$ was used to assess the phenomenon of conductivity decay induced by nitrophenyl coupling to the NT surface. The best fit of the above equation gives a depercolation threshold Φ_c of 0.68 and a critical exponent t of 2.5 (Figure 9b). The macroscopic conductivity (constant σ_0)

was estimated 78.4 S/m. Prior to the functionalization of the quarter nanotube sidewalls, carbon double bonds and nanoscale contacts are numerous enough to maintain high conductivity. The initial (13.5 S/m) and half-way conductivity differ by a factor of about 100. Close to Φ_c , more than 30% of the total number of double bonds is disrupted, and the conductivity loses again 75 times of its recently attained value. The lattice hosts more p-nitrophenyl functional groups covalently bonded to the carbon atoms and becomes 32:68 – $sp^3:sp^2$ -hybridized. This corresponds to the maximal functionalization. Lower conductivities could not have been attained, however, due to experimental and perhaps theoretical limitations. Theoretical calculation predicts a limit of functionalization around 71 wt.% (1 NP per double bond) (see equation S2 in supplementary information). At more extreme excess of injected reactant, the highest obtained functional degree was 61 wt.% within experimental error, which likely means that we are in the slow growth region of the sigmoidal function $\sigma = f(n(\text{DB-remaining}))$. The induced steric hindrance by many grafted NPs and the decrease on the reactivity of pre-functionalized SWNTs vs. NP reactivity with the functionalization progression could prohibit further functionalization beyond. Another suggested hypothesis is that, at 71 wt.%, no more NT pi electrons are available to be extracted in reaction with 4-nitrobenzenediazoether. These hypotheses are concordant with literature when small and very reactive functionalization agent such as fluorine is used.[30] The strong correlation between the functionalization limit and depercolation threshold of double bonds reinforces the latter hypothesis: super-functionalization stops because of the lack of delocalized electrons in extremely functionalized SWNTs.

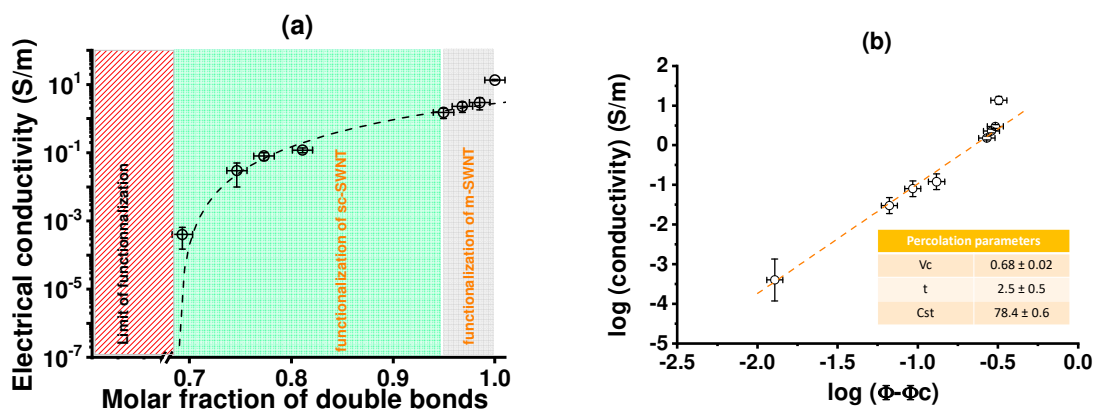


Figure 9. (a) Depercolation curve obtained after progressive functionalization. Grey zone represents the functionalization of m-SWNT, green zone the functionalization of sc-SWNT and red zone the limit of functionalization: A strong decrease in conductivity is associated to a gradual loss of C-C double bonds. (b) Modeling conductivity in a log-log plot as a function of the double bond content using Kirkpatrick's percolation law.

2.7. Electrochemical properties and energy levels

With a strong grasp of Raman-based knowledge on the influence of nitrophenyl functional groups toward the introduction of sp^3 carbon bonding sites, NP-SWNTs were electrochemically investigated for bandgap and energy levels. Such experiment was carried using the ferrocene/ferrocenium (Fc/Fc⁺) redox couple (4.80 eV below vacuum level) versus Ag/AgCl at a scan rate of 20 mV/s.

All materials were scanned twice and only the second voltammogram is presented for each analyzed sample in Figure S5 in the Supplementary Information. SWNTs exhibit no electrochemical characteristic signature between -3.5 and +3.5V. On the other hand, analysis of the voltammetric peaks of NP-SWNTs shows important oxidation (E_{ox}) and reduction peaks (E_{red}) that increase or decrease in response to the degree of functionalization. This variation allows us to calculate, for every NP-SWNT-X, the approximate HOMO and LUMO level (Figure 10) using the method detailed in Supplementary Information. The bandgap was concluded *via* calculating the difference between the two levels. Bandgap E_g and position of the energy levels of pristine SWNTs were extracted from literature reports.[38]

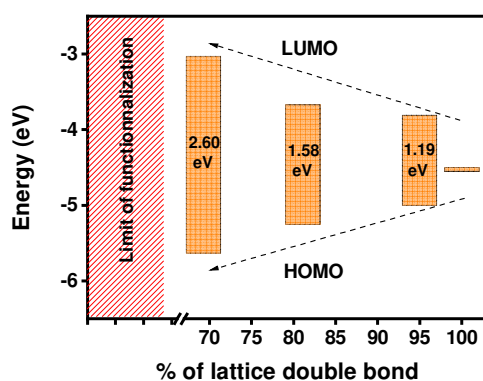


Figure 10. Concluded energy levels and electrochemical bandgaps of NP-SWNT-21, NP-SWNT-49 and NP-SWNT-61.

Table 2. Electrochemical properties (oxidation potential, reduction potential, HOMO, LUMO and band gap) obtained from NP-SWNT-X films drop-casted on platinum electrode.

| | | E_{ox} (V) | E_{red} (V) | E_{HOMO} (eV) | E_{LUMO} (eV) | E_g (eV) |
|----------------------|------------|--------------|---------------|-----------------|-----------------|------------|
| Functionalized SWCNT | NP-SWNT-21 | 0.27 | -0.92 | -5.00 | -3.81 | 1.19 |
| | NP-SWNT-49 | 0.52 | -1.06 | -5.25 | -3.67 | 1.58 |
| | NP-SWNT-61 | 0.90 | -1.70 | -5.63 | -3.03 | 2.60 |

It should be noted that even though there is insufficient information on the electrochemistry of functionalized CNTs, it is likely that our results are in deep coherence with a study conducted by Gross and Hickner[39] on bandgap modulation of NP-SWNTs and BrP-SWNTs (bromophenyl-SWNTs) using cyclic voltammetry.[40] Bandgaps calculated for NP-SWNT in this study range between 1.19 and 2.60 eV. It is also interesting to note that attaining the metallic threshold is necessary for the bandgap to appear. NP-SWNT-14 showed an $ID/IG = 0.1$ but no change in the cyclic voltammetric behavior. This is due to the fact that m-SWNTs should be completely functionalized to become visible in the CV probing.[39] Otherwise, their bandgap = 0 eV and they are not recognized. Gross and Hickner highlighted the presence of a threshold to change the band gap, but haven't quantitatively identified it. Superfunctionalization induces larger bandgaps as the conjugation length decreases and sp^3 defects become more numerous.

Apart from that, nitrophenylation of SWNTs brings to mind the opposite strategy employed in the engineering of low bandgap or π -conjugated polymers,[41, 42] where starting units are polymerized together

to increase the number of double bonds and boost conjugation. The bandgap becomes lower at the end; the electrochemistry of compounds and the optical absorption is strongly influenced. Similarly to nitrophenylation, the hydrogenation of graphene sheets toward graphane (which exhibits a large band gap) [43] provided interesting electrochemical [44] and electronic [45] properties.

3. Experimental

3.1. Superfunctionalization of SWNTs by Z diazoether and spectroscopic characterization

Our method of functionalization was carried out under ambient atmosphere in aqueous media. A schematic depiction of the reaction described below can be found in Figure S1 in Supplementary Information. In brief, RN-220 (Raymor NanoIntegris) SWNTs (diameter: 0.9-1.5 nm) were suspended at 2g/L in CTAB 0.2%, sonicated in an ice bath at 425 watt during 30 minutes, and centrifuged for 6 hours at 15000 g and 18 °C (in order to remove the catalyst residual). The upper supernatant was pipetted, buffered at pH 1 by the addition of phosphoric acid and treated by 3-o-p-nitrobenzenediazoascorbic acid, a mixture of 4-nitrobenzenediazonium tetrafluoroborate (NBDT) salt and ascorbic acid dissolved in cold water. To avoid rapid conversion of Z into E diazoether, the temperature of the solution was maintained throughout the experiment using an ice bath. Next, the solution was allowed to stir for 30 minutes and then UV-Vis spectrum was recorded. The reaction progress was monitored spectroscopically by following the evolution of the E isomer. The exact amount of ascorbate diazoether injected to shut the absorption of m-SWNTs in solution was designed as xI and used as reference for seven samples, each sample received higher or lower reagent quantities. We recognized that beyond xI , other absorption intensities are quantity dependent and took steps to quantify the successive decay in S^{22} peak. Spectra became featureless after adding 8-times the initial reactant amount. Here aggregation takes place, and SWNT absorption could no more be instantly followed. The rest of solution was precipitated in ethanol to remove the diazoether by-products and excessive surfactant, filtered under vacuum, and washed with copious amounts of ethanol, water and acetone. Metallic (15,0) and semiconducting (16,0) chiralities

were selected for the calculations, as their respective diameters of 1.19 and 1.27 nm are comparable to the average diameter of the SWNTs used in the experimental part of this study (1.2 nm)

3.2. UV-Vis-NIR spectroscopy

Solution absorption spectra were collected on a UV-1800 Shimadzu spectrophotometer in a 1 mm quartz cuvette from 200 to 1100 nm relative to reference cells containing CTAB surfactant or DMF according to the sample composition. Similarly, spectra of thin films were obtained on thin films casted from dilute SWNT/DMF solutions (0.1 g/L) on quartz substrates.

3.3. TEM observations

Samples for observations were ultrasonically dispersed in isopropanol for 3 minutes. A drop of the suspension was dried on 300 mesh copper grid and coated with holey carbon film. The TEM measurements of SWNTs were taken with a transmission electron microscope JEOL 2011 operating at 200 kV with a 0.19-nm point-to-point resolution.

3.4. SEM observations

Scanning electron microscopy was conducted on CNT films deposited on conductive ITO substrates at 30 kV. The sample was fixed on the support using a conductive carbon tape. Silver paste was coated on top of the sample in order to guarantee some conductivity and reduce the charging effect of the electron beam. The images were acquired using a SEM, model Zeiss Gemini 500. Many images (at least 5 per sample) have been taken to address the representativeness issues. The amount of grafting could be verified easily with a blind test.

3.5. Conductivity and electrochemical impedance spectroscopy

Both I-V characteristics and EIS spectra were collected using a Biologic Science instrument-SP 300 and data treated with EC-Lab software. Measurements covered a 1Hz-1MHz frequency range with a 2-probe method using Al electrodes at an applied voltage of 100 mV.

For preparation of the samples, a specific assembly procedure was developed. [46] In our configuration, both electrodes of aluminum should be deposited on the target buckypaper. For that the solid samples were assembled with an adhesive mask with pattern “window” of 1x2mm² to delimit the surface of cathode (in comparison to the anode surface). On each sample window, a buckypaper with thickness = 10-20 μm (measured by profilometer) and area $\approx 2 \times 3 \text{ mm}^2$ (measured by optical microscopy) was assembled. Finally, metallic contacts based on 200 nm of aluminium layer were deposited on each face using Joule effect evaporation in vacuum chamber. Configurations based on Al/SWNT/Al or AL/NP-SWNT-X/Al were obtained and characterized.

3.6. Raman spectroscopy

We measured Raman spectra of purified and functionalized SWNT films using a Bruker-Senterra Raman spectrometer with 532 nm excitation laser source. Signals were acquired from small regions of dried samples casted on quartz substrates, using 50 s accumulation time and 2 mW power. Our spectra are normalized to the dominant G-band peak near 1590 cm^{-1} . No baseline correction was brought to spectra unless otherwise stated.

3.7. FT-IR spectroscopy

FT-IR spectra of the produced CNT buckypapers were collected in attenuated total reflection (ATR) mode by Perkin Elmer Spotlight 400 FT-IR Imaging system between 600 and 4000 cm^{-1} with a resolution of 4 cm^{-1} .

4. Conclusions

Through accurate spectroscopic monitoring (UV-Vis-NIR and Raman), we experimentally illustrate the influence of custom functionalization on bulk-phase properties of SWNTs. We show that these nanoparticles, known for high conductivity and manipulation difficulty, can now be controllably switched to semiconductor printable films. This triggered semiconductivity could serve as the foundation for semiconducting SWNTs at the macroscopic level. CNTs functionalized for only m-nanotubes are still metals in conductivity. An offset among our functionalized samples is estimated to be a factor of ~ 34000 greater for pristine nanotubes as compared to those with 15-16 NP groups attached per 100 carbon atoms. Comparative studies on NT films before and after functionalization were illustrated, so that the dependence of both electrical and optical properties on electronic structure and chemical modification was determined. In line with such dependence, the experimental findings also reveal the quantitative variation with functionalization density of the Raman D/G intensity ratio, and a larger bandgap. Our model further shows that the intra-depercolation is achieved when NP functionals couple to $\sim 32\%$ of sp^2 -hybridized carbon lattice. The functionalization limit of this reaction, reflects the lack of sufficient delocalized π electrons to initiate nitrophenyl coupling. It remains a striking confirmation for the fact that the nitrophenyl coupling revolves mainly around the electron density of SWNTs and, in a deep coherence with the previous findings, makes it easier to understand the selectivity to metallic SWNTs. We think that the higher electron density was at the origin of the kinetically favored electron transfer from m-SWNTs towards the electrophilic ascorbate diazoether. Such an electron density fades gradually as the reaction proceeds due to the decrease in conjugation length. This initial evidence of gradual reactivity provides a handle for separation of these species. The strong correlations between the structure and electronic/optical properties of SWNTs functionalized covalently with nitrophenyl groups, emphasize

that molecular geometry controls the spatial distribution of charge density. This type of on-demand conductivity may find applications in, for example, nanotube sorting, selective sensors and optoelectronic devices. The examples described here demonstrate that the chemistry of this class of NP-functionalized single walled carbon nanotubes is just beginning. The basis for the exploitation of macroscopic quantities relative to the bulk phase like optical and electronic properties has been laid. The unique properties of SWNTs can now be coupled to adjusted conductivity to make use in combination with other classes of material whose properties are almost compatible.

Supplementary Information. Reaction scheme, additional spectral data, viscosity, equations, oxidation-reduction cyclic voltammograms and further calculations.

Acknowledgement

This work was performed within the framework of the Centre of Excellence of Multifunctional Architected Materials "CEMAM". The authors thank Jonathan Outin from Université Savoie Mont Blanc for the provision of the equipment/accessories required for the centrifugation experiments.

References

1. Iijima, S., *Helical microtubules of graphitic carbon*. *nature*, 1991. **354**(6348): p. 56.
2. Baughman, R.H., A.A. Zakhidov, and W.A. De Heer, *Carbon nanotubes--the route toward applications*. *science*, 2002. **297**(5582): p. 787-792.
3. Gabay, T., et al., *Electro-chemical and biological properties of carbon nanotube based multi-electrode arrays*. *Nanotechnology*, 2007. **18**(3): p. 035201.
4. Combessis, A., et al., *Understanding dynamic percolation mechanisms in carbonaceous polymer nanocomposites through impedance spectroscopy: Experiments and modeling*. *Journal of Applied Physics*, 2014. **116**(3): p. 034103.
5. Malara, F., et al., *A free-standing aligned-carbon-nanotube/nanocomposite foil as an efficient counter electrode for dye solar cells*. *Energy & Environmental Science*, 2012. **5**(8): p. 8377-8383.
6. Tune, D.D. and J.G. Shapter, *The potential sunlight harvesting efficiency of carbon nanotube solar cells*. *Energy & Environmental Science*, 2013. **6**(9): p. 2572-2577.
7. Holt, J.M., et al., *Prolonging charge separation in P3HT– SWNT composites using highly enriched semiconducting nanotubes*. *Nano letters*, 2010. **10**(11): p. 4627-4633.
8. Umeyama, T. and H. Imahori, *Carbon nanotube-modified electrodes for solar energy conversion*. *Energy & Environmental Science*, 2008. **1**(1): p. 120-133.
9. Jariwala, D., et al., *Carbon nanomaterials for electronics, optoelectronics, photovoltaics, and sensing*. *Chemical Society Reviews*, 2013. **42**(7): p. 2824-2860.
10. Diao, S., et al., *Chirality enriched (12, 1) and (11, 3) single-walled carbon nanotubes for biological imaging*. *Journal of the American Chemical Society*, 2012. **134**(41): p. 16971-16974.
11. Tanaka, T., et al., *High-yield separation of metallic and semiconducting single-wall carbon nanotubes by agarose gel electrophoresis*. *Applied physics express*, 2008. **1**(11): p. 114001.
12. Arnold, M.S., et al., *Sorting carbon nanotubes by electronic structure using density differentiation*. *Nature nanotechnology*, 2006. **1**(1): p. 60.
13. Arnold, M.S., S.I. Stupp, and M.C. Hersam, *Enrichment of single-walled carbon nanotubes by diameter in density gradients*. *Nano Letters*, 2005. **5**(4): p. 713-718.
14. Tanaka, T., et al., *Simple and scalable gel-based separation of metallic and semiconducting carbon nanotubes*. *Nano Letters*, 2009. **9**(4): p. 1497-1500.
15. Kanungo, M., et al., *Suppression of metallic conductivity of single-walled carbon nanotubes by cycloaddition reactions*. *Science*, 2009. **323**(5911): p. 234-237.
16. LeMieux, M.C., et al., *Self-sorted, aligned nanotube networks for thin-film transistors*. *Science*, 2008. **321**(5885): p. 101-104.
17. Chakraborty, A.K., K.S. Coleman, and V.R. Dhanak, *The electronic fine structure of 4-nitrophenyl functionalized single-walled carbon nanotubes*. *Nanotechnology*, 2009. **20**(15): p. 155704.
18. Nair, N., et al., *A Structure– Reactivity relationship for single walled carbon nanotubes reacting with 4-hydroxybenzene diazonium salt*. *Journal of the American Chemical Society*, 2007. **129**(13): p. 3946-3954.
19. Bahr, J.L. and J.M. Tour, *Covalent chemistry of single-wall carbon nanotubes*. *Journal of Materials Chemistry*, 2002. **12**(7): p. 1952-1958.
20. Bahr, J.L., et al., *Functionalization of carbon nanotubes by electrochemical reduction of aryl diazonium salts: a bucky paper electrode*. *Journal of the American Chemical Society*, 2001. **123**(27): p. 6536-6542.
21. Dyke, C.A. and J.M. Tour, *Solvent-free functionalization of carbon nanotubes*. *Journal of the American Chemical Society*, 2003. **125**(5): p. 1156-1157.
22. Ngoc, Q.B.V., M.-S. Choi, and W.-J. Kim, *A simple quantitative estimate of the number of functional groups on the surfaces of single-walled carbon nanotubes*. *RSC Advances*, 2016. **6**(8): p. 6451-6458.
23. Schmidt, G., et al., *Mechanism of the coupling of diazonium to single-walled carbon nanotubes and its consequences*. *Chemistry-A European Journal*, 2009. **15**(9): p. 2101-2110.
24. Strano, M.S., et al., *Electronic structure control of single-walled carbon nanotube functionalization*. *Science*, 2003. **301**(5639): p. 1519-1522.
25. Darchy, L., et al., *A highly selective non-radical diazo coupling provides low cost semi-conducting carbon nanotubes*. *Carbon*, 2014. **66**: p. 246-258.
26. Hugot, N., et al., *Gram-scale carbon nanotubes as semiconducting material for highly versatile route of integration in plastic electronics*. *physica status solidi (a)*, 2016. **213**(1): p. 183-192.
27. Powell, L.R., M. Kim, and Y. Wang, *Chirality-Selective Functionalization of Semiconducting Carbon Nanotubes with a Reactivity-Switchable Molecule*. *Journal of the American Chemical Society*, 2017. **139**(36): p. 12533-12540.

28. Cabana, J. and R. Martel, *Probing the reversibility of sidewall functionalization using carbon nanotube transistors*. Journal of the American Chemical Society, 2007. **129**(8): p. 2244-2245.
29. López-Bezanilla, A., et al., *Effect of the chemical functionalization on charge transport in carbon nanotubes at the mesoscopic scale*. Nano letters, 2009. **9**(3): p. 940-944.
30. Mickelson, E., et al., *Fluorination of single-wall carbon nanotubes*. Chemical physics letters, 1998. **296**(1-2): p. 188-194.
31. Ghosh, S., et al., *Structure-Dependent Thermal Defunctionalization of Single-Walled Carbon Nanotubes*. ACS nano, 2015. **9**(6): p. 6324-6332.
32. Saito, R., G. Dresselhaus, and M.S. Dresselhaus, *Physical properties of carbon nanotubes*. 1998: World Scientific.
33. Bekyarova, E., et al., *Chemical Modification of Epitaxial Graphene: Spontaneous Grafting of Aryl Groups*. Journal of the American Chemical Society, 2009. **131**(4): p. 1336-1337.
34. Combessis, A., L. Bayon, and L. Flandin, *Effect of filler auto-assembly on percolation transition in carbon nanotube/polymer composites*. Applied Physics Letters, 2013. **102**(1): p. 011907.
35. Badard, M., et al., *Optimization and control of dynamic percolation in nanostructured silicon oils*. The European Physical Journal Applied Physics, 2017. **79**(1): p. 10401.
36. Stauffer, D. and A. Aharony, *Introduction to percolation theory*. 1994: CRC press.
37. Kirkpatrick, S., *Percolation and conduction*. Reviews of modern physics, 1973. **45**(4): p. 574.
38. Jeon, I., et al., *Single-walled carbon nanotube film as electrode in indium-free planar heterojunction perovskite solar cells: investigation of electron-blocking layers and dopants*. Nano letters, 2015. **15**(10): p. 6665-6671.
39. Gross, M.L. and M.A. Hickner, *Using Cyclic Voltammetry to Measure Bandgap Modulation of Functionalized Carbon Nanotubes*. Electrochemical and Solid-State Letters, 2010. **13**(2): p. K5-K7.
40. Wilder, J.W., et al., *Electronic structure of atomically resolved carbon nanotubes*. Nature, 1998. **391**(6662): p. 59.
41. Gutzler, R., *Band-structure engineering in conjugated 2D polymers*. Physical Chemistry Chemical Physics, 2016. **18**(42): p. 29092-29100.
42. Ashraf, R.S., et al., *Thienopyrazine-Based Low-Bandgap Poly(heteroaryleneethynylene)s for Photovoltaic Devices*. Macromolecular Rapid Communications, 2006. **27**(17): p. 1454-1459.
43. Pumera, M. and C.H.A. Wong, *Graphane and hydrogenated graphene*. Chemical Society Reviews, 2013. **42**(14): p. 5987-5995.
44. Ambrosi, A., et al., *Electrochemistry of graphene and related materials*. Chemical reviews, 2014. **114**(14): p. 7150-7188.
45. Zhang, H., et al., *Aryl Functionalization as a Route to Band Gap Engineering in Single Layer Graphene Devices*. Nano Letters, 2011. **11**(10): p. 4047-4051.
46. Nourdine, A., et al., *Extrusion of a nano-ordered active layer for organic photovoltaic cells*. Sustainable Energy & Fuels, 2017. **1**(9): p. 2016-2027.